This is a preprint, the final version is subject to change, of the American Mineralogist (MSA)
Cite as Authors (Year) Title. American Mineralogist, in press.
DOI: https://doi.org/10.2138/am-2018-6314

Temperature dependence of Raman shifts and linewidths for Q^0 and Q^2 crystals of silicates, phosphates and sulfates

Revision 2 (Ms 6314)

H. Wayne Nesbitt[a], G. Michael Bancroft[b], and Grant S. Henderson[c]

[a] **Department of Earth Sciences, Univ. of Western Ontario, London, Canada**

[b] **Department of Chemistry, Univ. of Western Ontario, London, Canada**

[c] **Dept. of Earth Science, Univ. of Toronto, Toronto On., M5S 3B1, Canada**

Corresponding Author: H. Wayne Nesbitt, Tel: (519) 661-2100 ext. 83194, e-mail:hwn@uwo.ca

Keywords: Raman Shifts in crystals, Raman Linewidths in crystals, Temperature dependence of Raman Shifts, Temperature dependence of Raman linewidths.

This is a preprint, the final version is subject to change, of the American Mineralogist (MSA)
Cite as Authors (Year) Title. American Mineralogist, in press.
DOI: https://doi.org/10.2138/am-2018-6314

ABSTRACT

The temperature dependence of Raman shifts and linewidths (full width at half maxima or FWHM) for the A_1 symmetric stretch of TO_4 (T= Si, P, S) have been analysed for 9 alkali and alkaline earth silicates, phosphates and sulfates. In crystalline silicates, the Q^0 and Q^2 species Raman shifts decrease with temperature, whereas FWHM increase. The *strikingly similar* behaviour of Q^0 and Q^2 in silicates and Q^0 in phosphates makes it possible to estimate to within ± 4 cm^{-1} Raman shifts up to ~1000 K. Similarly systematic increases in FWHM with temperature can be estimated to within ± 5 cm^{-1} up to ~1400 K. The type of element centering TO_4 (i.e., Si, P, or S) has *no appreciable effect* on the temperature dependence of Raman shifts or linewidths; the local environment of the Q^0 and Q^2 tetrahedra is the primary determinant of the temperature dependence. The type of cation in the first coordination sphere of the tetrahedron may have a secondary effect by affecting Heisenberg lifetimes of Raman virtual states.

Previous theoretical considerations have been modified to include the effect of the Heisenberg (or natural) lifetime on Raman FWHM. This contribution is required to explain the anomalous FWHM of Li_2SiO_3 relative to the FWHM of isostructural Na_2SiO_3 and the large Li_2SO_4 and Li_3PO_4 FWHM (relative to Ba and Sr phosphates). The theoretically based expressions dictate a necessary, simple relationship among temperature, Raman shift and FWHM. The relationship is developed and it allows, with one measurement of Raman shift and FWHM (e.g., measured at 298 K), prediction of Raman shifts *and* FWHM of Q^0 and Q^2 crystals to within 5 cm^{-1} up to ~1500 K. The properties of the TO_4 moiety (T = Si, P, S) are mostly responsible for the striking regularity of Raman shifts and FWHM, although alkali and alkaline earth cations affect to varying extent Heisenberg lifetimes, hence FWHM.

INTRODUCTION

The Raman spectra of crystals in the region 800-1200 cm^{-1} (i.e., the A_1 TO_4 symmetric stretching mode) commonly display a prominent, narrow Lorentzian peak with a well defined position at room temperature. The best documented data on crystalline silicate Raman shifts and linewidths are provided by Richet et al. (1996; 1998) who present data for Li_2SiO_3, Na_2SiO_3, $CaSiO_3$ and $Ca_{0.5}Mg_{0.5}SiO_3$ metasilicate crystals from 298 K to their melting points. These crystals have different structures but all consist of Si tetrahedra where each Si center is bonded to two bridging oxygen atoms (BO or Si-O-Si) and two non-bridging oxygen atoms (NBO or e.g., Si-O-Na). These are referred to as Q^2 species (Q indicates a Si center and the superscript indicates the number of BO atoms per tetrahedron). In addition, numerous papers provide reasonably well characterized data (in graphical form) on Raman shifts and linewidths for crystals containing Q^0 species, including silicates, phosphates and sulfates (Cazanelli and Frech, 1984; Popovic et al., 2003; Kolosev and Geiger, 2004; Zhai et al., 2011; 2014). These data have been inspected and where feasible Raman shifts and linewidths have been evaluated. After studying the data we arrive at two major questions concerning the spectra of crystals. *First*, do Raman shifts and FWHM of the Q species describe similar trends as a function of temperature or do they describe unique trends in temperature, each trend being dependent on crystal structure and composition? *Second*, can the temperature dependence of the Raman shifts and FWHM be explained using existing theories? Our goals are to answer these questions. There has been no comprehensive study relating these two temperature dependent spectral properties for silicates, phosphates or sulfates and few on other materials (e.g., Klemens, 1966; Liu et al., 2000). Our most important observation is that the temperature dependence of Raman shifts and FWHM predicted from theory is observed for experimental data. Moreover, Raman shifts or FWHM can

be reasonably estimated at high temperature provided the temperature dependence of the other is known.

Richet et al. (1996; 1998) demonstrated that the Raman linewidths and peak shapes change within the premelting regions of the Q^2 crystals Na_2SiO_3, Li_2SiO_3 and $CaSiO_3$ and Nesbitt et al. (2017a) interpreted the changes in these spectra to result from introduction of a Q^3 band to the Raman spectra. The interpretation would have been tenuous had not Richet et al. (1998; 1996) demonstrated that the Raman shift and linewidths of the Q^2 band changed systematically with temperature. These systematics now can be calculated by theoretical means here outlined allowing prediction of Raman shifts and linewidths at temperatures where experimental studies are difficult. An important aspect of the theory is the quantification of 'constants' of the equations utilized. These constants relate to fundamental properties of crystals, glasses and melts, such as thermal expansion, the Grüneisen parameter (McMillan and Wolfe, 1995), and the relative importance of harmonic and anharmonic contributions to Raman shifts and linewidths. Thus Raman spectral measurements can be related directly to other fundamental properties of crystals, glasses and melts.

Theoretical aspects developed by Balkanski et al. (1983) relate directly to the temperature dependence of Raman shifts and linewidths. The linewidths of some crystals are appreciably broader than others at ambient temperature, and the linewidths of glasses are still broader than those of crystals for equivalent composition (Richet et al., 1996; 1998). As proposed here, broad Raman bands are the result of short Heisenberg lifetimes of Raman virtual states (see also Bancroft et al., 2018). The theory of Balkanski et al. (1983) has been expanded to include Heisenberg lifetimes. In addition, Raman shifts are dependent on thermal expansion and the Grüneisen parameter (McMillan and Wolfe, 1995), and the theory may be used to gain insight

into these parameters for crystals, glasses and melts over a wide range of temperature. An understanding of these aspects begins with a reasonable theory such as that of Balkanski et al. (1983). Here we demonstrate that their theory, modified to include Heisenberg (natural) lifetimes, may be used to address these aspects.

Summary of Theory

Several papers discuss theoretical aspects of temperature dependences of Raman shifts and FWHM of elemental solids such as silicon and diamond, and of alloys (e.g., Klemens, 1966; Hart et. al. 1970; Balkanski et al., 1983; Menéndez and Cardona, 1984; Burke and Herman, 1993; McMillan and Wolfe, 1995; Cui et al., 1998; Liu et al., 2000). Theoretical considerations of temperature dependence begin with the classical anharmonic oscillator where the potential energy (V_s) is described by an expansion in 'x', which is the displacement of the oscillator from its equilibrium position (e.g., Hart, 1970):

$$V_s = ex^2 + fx^3 + gx^4 + \quad (1)$$

where e, f and g are constants. The quadratic term represents the potential energy associated with a harmonic oscillator. The cubic term gives rise to thermal expansion and is partially responsible for the *temperature dependence* of Raman shifts and FWHM of Raman spectra (e.g., Hart, 1970; Balkanski et al., 1983). The quartic term reflects large amplitude vibrational weakening. In the anharmonic approximation, the fundamental Raman shift (ω^*) or alternatively the zone-center unperturbed frequency (Liu et al., 2000) consists of a real and an imaginary part. Both parts are temperature dependent with the real part, the Raman shift, decreasing in frequency with temperature and the imaginary part, the linewidth, increasing (Liu et al., 2000).

The equations that follow relate to zone centers of a crystal (Balkanski et al., 1983; Nishidate and Sato, 1992; Burke and Herman, 1993; Sato and Asari, 1995; Cui et al., 1998; Liu

et al., 1999; Liu et al., 2000; Moura et al., 2016). From the treatment of Balkanski et al. (1983) the equation for the temperature dependence of the Raman shift at temperature ($\Omega(T)$) is:

$$\Omega(T) = \omega^* + C[1 + 2/(e^x - 1)] + D[1 + 3/(e^y - 1) + 3/(e^y - 1)^2] \quad (2)$$

C and D are constants and include the coefficient of thermal expansion and the Grüneisen parameter (McMillan and Wolfe, 1995). The constant ω^* is the fundamental (or Einstein) frequency of the Raman oscillator at absolute zero. Also, $x = h\omega^*/2kT$ and $y = h\omega^*/3kT$, where h is Planck's constant, k is Boltzmann's constant, and $h\omega^*/k$ is the Einstein temperature (θ_E) for the Raman oscillator. The terms $2/(e^x - 1)$ and $3/(e^y - 1)$ are closely related to the average energy of the Raman oscillator (ε_R) at thermal equilibrium (i.e., $\varepsilon_R = h\omega^*/(e^{h\omega^*/kT} - 1)$, Omar 1975, p. 76-77). Expansion of Equation (2) and collection of constants yields:

$$\Omega(T) = \Omega^* + C[2/(e^x - 1)] + D[3/(e^y - 1) + 3/(e^y - 1)^2] \quad (3)$$

where Ω^* is the Raman shift at absolute zero and is equal to ω^*+C+D; it is the Raman shift in the 'harmonic limit' (i.e., arises from the quadratic term of Eq. 1). As shown subsequently, the numerical values for C and D are less than 10 whereas values for ω^* are very large so that $\Omega^* \sim \omega^*$ (e.g., ω^* ~950-1000 cm^{-1} for the Q^2 symmetric stretch in chain silicates). The second and third terms on the right-hand side of Equation (3) are the cubic and quartic contributions which give rise to the non-linear temperature dependence of Raman shifts (Ω). Balkanski et al., (1983) also provided an equation for the temperature dependence of FWHM:

$$FWHM(T) = A[1 + 2/(e^x - 1)] + B[1 + 3/(e^y - 1) + 3/(e^y - 1)^2] \quad (4)$$

where FWHM(T) is the linewidth at temperature T and A and B are constants. Other terms are as for Equation (2). Expansion of the equation and collection of the constants yields:

$$FWHM(T) = FWHM^* + A[2/(e^x - 1)] + B[3/(e^y - 1) + 3/(e^y - 1)^2] \quad (5)$$

where FWHM* is the linewidth at absolute zero and is equal to A+B (e.g., Liu et al., 2000, their

Eq. 3). Balkanski et al. (1983) did not consider the lifetime effect of the Raman virtual state (excited or intermediate state) and it must be included if their treatment is to apply to phases whose natural (or Heisenberg) lifetimes are short. The Heisenberg lifetime ($FWHM^H$) is given by the Heisenberg uncertainty principle (e.g., Adamson, 1973, p. 742):

$$FWHM^H = k/t^{1/2} \quad (6)$$

where k is a constant and $t^{1/2}$ is the half-life of the Raman virtual state. The shorter the lifetime of the virtual state (i.e., the smaller the value of $t^{1/2}$) the greater the FWHM of the Raman line. Virtual states with long lifetimes yield effectively a constant, minimum linewidth (FWHM*). For short lifetimes $FWHM^H > FWHM^*$ so that:

$$FWHM^H = FWHM^* + \Delta FWHM^H \quad (7)$$

where $\Delta FWHM^H$ is the difference between $FWHM^H$ and FWHM*. The corrected form of Equation (5) is:

$$FWHM(T) = FWHM^H + A[2/(e^x - 1)] + B[3/(e^y - 1) + 3/(e^y - 1)^2] \quad (8a)$$

or

$$FWHM(T) = FWHM^* + \Delta FWHM^H + A[2/(e^x - 1)] + B[3/(e^y - 1) + 3/(e^y - 1)^2] \quad (8b)$$

where FWHM* and $\Delta FWHM^H$ are constants for a given crystal. With our present state of understanding, the constants ω*, A, B, C and D must be evaluated from experimental data, although ω*can be reasonably well estimated from the Raman shift of a Q species. The constants are treated subsequently as fit parameters and their numerical values are evaluated by fitting Equations (2) and (8a) to data over appropriate temperature ranges.

Only Liu et al. (2000) report a direct relationship between Raman shifts and FWHM (for diamond) as a function of temperature. The circumstance is surprising because the cubic and quartic terms of Equations (2) and (4 or 8) are the same (coefficients excepted). The data

158 collected here provide an opportunity to test Equations (2) and (4 or 8), and to investigate the
159 relationship between Raman shift and FWHM as a function of temperature. Our findings also
160 allow assessment of the effects of crystallographic properties and long-range electrostatic
161 (cation-SiO_4) interactions on the numeric values of constants incorporated into the equations.

162 Our approach is useful because the temperature dependence of the FWHM and Raman
163 shifts generally have been unsuccessful where evaluated from first principles by calculating the
164 phonon dispersion curves across the Brillouin zone of crystals, using site potential energies
165 which include cubic and quartic terms (MgF_2 – Nishidate and Sato, 1992); α-$GaPO_4$ – Nakamura
166 et al., 1990; SnO_2 – Sato and Asari, 1995; $PbMoO_4$ – Sinagawa et al., 2000; $PbWO_4$ – Suda et
167 al., 2014); β-$(AlGa)_2O_3$ thin films – Wang et al., 2016; β-Ag_2MoO_4 – Moura et al., 2016). The
168 calculated phonon dispersion curves give an estimate of FWHM at a given temperature but as
169 shown for the symmetric Mg-F stretch of MgF_2, good agreement with the experimental FWHM
170 generally cannot be obtained (e.g., Nishidate and Sato, 1992). The exception is $PbMoO_4$
171 (Sinagawa et, 2000) where the temperature dependence of the shifts and FWHM were
172 successfully calculated from first principles.

173 ## DATA SOURCES AND ERRORS

174 ### Raman Shifts and FWHM from the Literature

175 All Raman shifts and FWHM in this paper come from previously published spectra.
176 Richet et al., (1996; 1998) tabulate values for crystalline Na_2SiO_3, Li_2SiO_3, $CaSiO_3$,
177 $Ca_{0.5}Mg_{0.5}SiO_3$ and associated errors probably are less than ±2 cm^{-1} for Raman shifts and
178 FWHM. We rely heavily on these data. Some results are derived from Raman shifts and FWHM
179 of published, large scale figures and the data have been accurately extracted by scanning and
180 digitizing the plots (Kolosev and Geiger, 2004; Popovic et al., 2003; Cazzanelli and Frech,

1984). Raman shifts or FWHM from these plots have associated errors of about ±2 cm^{-1}. For the phosphate crystals, $Sr_3(PO_4)_2$ and $Ba_3(PO_4)_2$ (Zhai et al., 2014), the FWHM have been extracted with an accuracy of about ±1 cm^{-1}. Unfortunately, Raman shifts for the two crystals cannot be utilized because they could not be accurately extracted from the small scale plots. In a few cases, Raman shifts and FWHM at 298 K and 1200 K were estimated from the published spectra (Voronko et al., 2015; You et al., 2001; Sadykov, 2004), and associated errors are ± 3-5 cm^{-1}.

FWHM: Instrumental Limits

Some crystals yield very narrow FWHM. For calcite ($CaCO_3$), the A_{1g} symmetric CO_3 stretch at 1086 cm^{-1} has a FWHM of ~0.5 cm^{-1} at <50 K and ~1.5 cm^{-1} at 300 K (Park, 1967). Similarly, the FWHM of crystalline SiF_4 is ~1 cm^{-1} at 77 K (Bernstein and Meredith, 1977) and is much narrower than any of the TO_4 symmetric stretches at 298 K. Raman spectroscopy therefore is capable of exceptionally high resolution and it must be concluded that FWHM of the TO_4 symmetric stretch observed for silicates, phosphates and sulfates are *not* instrumental in origin; the instrumental linewidth in all of these studies is less than 2 cm^{-1}.

INTERPRETATION OF RESULTS

Lineshape and Linewidths of Silicates

Individual Raman bands display fully Lorentzian lineshapes in the absence of other contributions (Loudon, 1963; Efimov, 1999). The major band of a α-cristobalite spectrum (Fig. 1a) and other SiO_2 polymorphs, (Fig. 1b) are narrow near the band maximum but are distinctly flared toward the band extremities. These are properties characteristic of Lorentzian peaks. A 98% Gaussian Voigt peak (2% Lorentzian) has been fit to the upper portion of the *low frequency side* of the band in Figure 1a. Although the upper portion of the peak is well fit, the flared extremity on the low frequency side is poorly fit. A second, 98% Lorentzian Voigt peak (2%

Gaussian) was fit in precisely the same manner. The major difference in the two fits is that the (mostly) Lorentzian peak fits well the flared portion of the band between ~410-350 cm-1; the α-cristobalite band is mostly Lorentzian in shape. There is, however, an additional contribution to the band which leads to asymmetry on the high frequency side of the band.

Raman shifts and FWHM for numerous crystalline silicates are summarized in Table 1. The silicate spectra usually consist of a prominent, narrow Lorentzian band with FWHM between ~4-13 cm^{-1} at 298 K (Richet et al., 1996; 1998). The bands arise from the A_1 symmetric SiO_4 stretch in all cases, although a small site symmetry splitting of the symmetric stretch is evident in four minerals of Table 1 (e.g., Kolosev and Geiger, 2004; Zucker and Shim, 2009). Each Q species here addressed is restricted to a narrow frequency range regardless of alkali or alkaline earth present (Table 1; see also Nesbitt et al., 2017b). From Table 1, FWHM ~9 (±4) cm^{-1} at 298 K and ~25 (±5) cm^{-1} at ~1200 K. Apparently, the FWHM for crystalline silicates are similar at a given temperature regardless of chemical composition or structure of the crystal.

Metasilicate Crystals

Q^2 Raman Shifts. The most intense Raman bands of the Q^2 crystalline silicates, Na_2SiO_3, Li_2SiO_3, $CaSiO_3$ and $Ca_{0.5}Mg_{0.5}SiO_3$, range from ~950-1000 cm^{-1} at 298 K (Richet et al., 1996; 1998; Nesbitt et al., 2017b) and their Raman shifts decrease systematically with temperature (Figs. 2a, 2b). With the Raman shifts standardized to the value at 298 K (Fig. 2c), the similarity in temperature dependence becomes obvious and although the Raman shifts of the crystals diverge somewhat with temperature, all remain within ~5 cm^{-1} at 1500 K. Equation (2) was used to fit the Raman shifts and the fit coefficients are listed in the figures. The solid curves represent best fits, the dashed curve the contribution of the $C[1 + 2/(e^x - 1)]$ term of Equation (2). The difference between the dashed and solid curves represents the contribution of the last term of

Equation (2). Both terms contribute significantly to the Raman shifts at temperature.

Equation (3) can be used to obtain the Raman shift at absolute zero (Ω^*) using the fit coefficients listed in Figures 2a and 2b (i.e., $\Omega^* = \omega^* + C + D$). This value may be used in turn to test the applicability of the Balkanski et al. (1983) theory to the metasilicate crystals. The Ω^* value calculated for Li_2SiO_3 is 977 cm^{-1}, for Na_2SiO_3 is 966 cm^{-1}, $CaSiO_3$ is 982 cm^{-1} and for $Ca_{0.5}Mg_{0.5}SiO_3$ is 1010 cm^{-1}. The Balkanski et al. (1983) theory predicts that Ω^* is similar to but a few wavenumbers less than the Raman shifts at 298 K (Table 1), as shown in Figure 2 by the near-flat trends of solid curves between 0 and 298 K. The theory and observation are consistent.

Li_2SiO_3 and Na_2SiO_3 are isostructural, having orthorhombic symmetry and consisting of Si_2O_6 chains with two BO per SiO_4 tetrahedron (Richet et al., 1996). Diopside, $Ca_{0.5}Mg_{0.5}SiO_3$, has monoclinic symmetry and is made up of Si_2O_6 chains whereas pseudowollastonite, $CaSiO_3$, is triclinic and consists of Si_3O_9 rings (Richet et al., 1998). Although the structures of these metasilicate crystals are different, the standardized Raman shifts (Fig. 2c) are similar indicating that Raman shifts do not depend substantially on the crystal structure or composition. This leaves the properties of the TO_4 tetrahedral bonds and the associated site potentials as the major factors controlling the temperature dependence of Raman shifts for Q^2 crystals.

Q^2 FWHM. As shown in Figures 3a and 3b, the FWHM of Na_2SiO_3, $CaSiO_3$ and $Ca_{0.5}Mg_{0.5}SiO_3$ increase systematically with temperature. Equation (8a) was used to fit these data and the fits are illustrated by the solid curves (Figs. 3a, 3b). These fits employed ω^* values derived from the fits to the Raman shift data (Fig. 2). The contributions from the second term (i.e., $A[1 + 2/(e^x - 1)]$ of Equation (8a) are illustrated by dashed curves of Figure 3a and the difference between the dashed and solid curves represents the FWHM contribution from the anharmonic (last) term of Equation (8a).

The linewidth of Li_2SiO_3 at 298 K is anomalously large compared with the FWHM (at 298 K) of isostructural Na_2SiO_3 (Fig. 3a). Equation (4) yields a poor fit to the FWHM of Li_2SiO_3 with FWHM(298 K) = 3.4 cm^{-1} and with the 'B' coefficient being negative producing a sigmoid fit and a maximum in FWHM (which has no physical meaning). The poor fit emphasizes the inadequacy of Equation (4), which lacks of a Heisenberg lifetime contribution. Equation (8a) was used to fit successfully the Li_2SiO_3 FWHM data. The best fit, using $\omega^* = 981.1$ (Fig. 2a), is illustrated in Figure 3a (fit coefficients listed in the figure). With $FWHM^H = 11.72$ cm^{-1} and $FWHM^* = A+B = 5.36$ cm^{-1} then $\Delta FWHM^H = 6.36$ cm^{-1}. We suggest that the virtual state of Li_2SiO_3 has a short natural lifetime leading to an elevated FWHM at 298 K relative to the FWHM of isostructural Na_2SiO_3 at 298 K (Fig. 3a).

The FWHM of the Q^2 silicate crystals were standardized to the value at 298 K (i.e., FWHM at T minus FWHM at 298 K) and the standardized FWHM have been plotted in Figure (3c). The FWHM values of Na_2SiO_3 above 1200 K (Fig. 2a) are affected by premelting (Richet et al., 1996; Nesbitt et al., 2017a) and have not been plotted. The standardized FWHM for the four crystals fall within ±3 cm^{-1} at any given temperature (Fig. 3c). The data has been fit as a group using Equation (5) and the solid curve of Figure 3c is the result. The FWHM*, A and B fit parameters are given in the figure. The fit reproduces remarkably well the standardized FWHM up to ~1500 K. Beyond this temperature, the Q^2 crystals containing Ca undergo Ca disordering and are subject to premelting phenomena (Dimanov and Ingrin, 1995; Richet et al., 1998; Dimanov and Jaul, 1998; Bouhifd et al., 2002; Nesbitt et al., 2018).

The similarity of the standardized FWHM values (Fig. 3c) is taken as evidence that different crystal structures and different alkali and alkaline earth elements have only minor effects on FWHM of the Q^2 silicate crystals. As with Raman shifts, the temperature dependence

of the Q^2 FWHM are controlled primarily by the properties of the TO_4 tetrahedra and associated site potentials; hence the Balkanski et al. (1983) formalism with a natural lifetimes included successfully reproduces the FWHM temperature trends. There is a strong negative correlation between the temperature dependence of the standardized Raman shift (Fig. 2c) and FWHM (Fig. 3c). The standardized shift decreases by about 30 cm^{-1} from 298 K to 1600 K, whereas the standardized FWHM increases by about 30 cm^{-1} over the same temperature range. The negative correlation has not been observed or explained before, and is addressed subsequently.

Orthosilicate Crystals

Forsterite Q^0 Raman Shift. The temperature dependence of the Q^0 Raman shift for Mg_2SiO_4 (Kolesov and Geiger, 2004) is illustrated in Figure (4a). The shifts decrease linearly with temperature indicating that the 'D' coefficient of Equation (2) is effectively 0.0 so that the quadratic term of Equation 1 dominates the Raman shifts of forsterite. The standardized Q^0 Raman shift of forsterite, the Q^2 shift of $CaSiO_3$ and Li_3PO_4 (Popovic et al., 2003, discussed subsequently), are plotted in Figure 4b. All decrease at a similar rate between 298 K and ~1000 K and they differ by about 3 cm^{-1} at 1200 K. Although not shown, the standardized Q^0 Raman shift of Mg_2SiO_4 is also similar to the Q^2 Raman shifts of the other metasilicates up to ~1000 K. Apparently, the temperature dependence of Q^0 and Q^2 Raman shifts of crystals are influenced by a property common to all Q^2 and Q^0 crystals, the TO_4 tetrahedra of the crystals. Composition and structure apparently have little influence on Raman shift temperature dependence of the Q^0 crystals. The linear temperature dependence above 298 K for the forsterite Q^0 Raman shift implies that harmonic oscillator properties alone affect the Raman shift. Anharmonic contributions produce a non-linear response in temperature and these apparently are minimal (i.e., 'D' of Eq. 3 is ~0). Higher temperature measurements are required to test the conclusion.

296 **Forsterite Q^0 FWHM.** The FWHM of the Q^0 band for Mg_2SiO_4 increases linearly with
297 temperature (Fig. 4c). The linear behaviour indicates that the B coefficient of Equations 4 and 8a
298 is effectively zero and that the quadratic term (i.e., $A[2/(e^x - 1)]$) controls temperature
299 dependence and as indicated by the dashed curves of Figure 3a this term is linear in T above 298
300 K. The FWHM of the Q^0 band for Mg_2SiO_4 and the Q^2 band for $CaSiO_3$ are similar up to ~1000
301 K (Fig. 4c) but they diverge at higher temperatures. Figure 4d illustrates FWHM values
302 standardized to the value at 298 K (i.e., FWHM(T)–FWHM(298)) for the Q^0 band of forsterite
303 and the Q^2 bands of the four metasilicates. All respond similarly to temperature up to ~1400 K.
304 Apparently the controls on the temperature dependence of Q^0 and Q^2 FWHM are effectively the
305 same to high temperature. Clearly the temperature dependence of these Q species linewidths do
306 not reflect crystal composition or structure. Moreover, the molecular symmetry of the two
307 tetrahedra (Q^0 and Q^2) differs as do site symmetries in the respective crystals. Apparently, the
308 temperature dependence of FWHM of the Q species of the crystals is controlled primarily by the
309 essential SiO_4 tetrahedral properties and little else.

310 **Q^0 of Sulfates and Phosphates.** The low temperature space groups for Li_2SO_4, Li_3PO_4,
311 $Sr_3(PO_4)_2$ and $Ba_3(PO_4)_2$ are $P2_1/b$, $Pmn2_1$, R^-3m, and R^-3m, respectively, with Li_2SO_4 and
312 Li_3PO_4 undergoing phase transitions at higher temperatures. The phosphate and sulfate spectra
313 contain only one symmetric Lorentzian peak which arises from the symmetric TO_4 (T = P, S)
314 stretch (Table 2). The Q^0 Raman shift of Li_2SO_4 decreases systematically with temperature to
315 ~840 K (Fig. 5a), where a monoclinic-fcc phase transition occurs (Cazzanelli and Frech, 1984).
316 The monoclinic and fcc *trends* display similar slopes and these are almost coincident with the
317 slope of the Q^2 Raman shift vs. temperature trend of Li_2SiO_3 (Fig. 5a). Apparently, neither
318 crystal structure nor composition (Si or S of tetrahedra) affects appreciably the *temperature*

319 *dependence* of the Raman shifts of the sulfate.

320 The Q^0 Raman shift vs. temperature trend for Li_3PO_4 (Popovic et al., 2003) is illustrated
321 in Figure 5b. Equation (3) was used to fit the data and the three fit parameters are listed in the
322 figure. Although the fit is good, it is not robust, primarily because the lowest temperature datum
323 point is at ~350 K and the trend of the 6 highest temperature points is offset from the trend of the
324 lower temperature data. Nevertheless, the Li_3PO_4 Q^0 Raman shift dependence on temperature is
325 similar to the Q^2 trend for Li_2SiO_3 up to ~1300 K. The standardized Raman shifts for Mg_2SiO_4,
326 Li_3PO_4, Li_2SO_4 and Li_2SiO_3 (Fig. 5c) behave similarly and are within ±2 cm^{-1} up to ~850 K (the
327 temperature at which Li_2SO_4 changes structure). These data demonstrate that the temperature
328 dependence of the Q^0 Raman shifts are largely independent of composition and structure of the
329 crystal and dependent primarily on the properties of the tetrahedron, whether SiO_4, PO_4 or SO_4.

330 The FWHM-temperature trends of Li_2SO_4, Li_3PO_4, $Sr_3(PO_4)_2$ and $Ba_3(PO_4)_2$ are
331 compared with that of Mg_2SiO_4 in Figure 6a. All incorporate Q^0 species and where standardized
332 to the value at 298 K (Fig. 6b), they display remarkably consistent trends with respect to
333 temperature. As shown in Figure (6c), their trends are also similar to $CaSiO_3$ which contains Q^2
334 species. Agreement between standardized Q^0 and Q^2 slopes is within ~2 cm^{-1} up to ~1400 K,
335 indicating a common control on the temperature dependence of the two Q species FWHM for
336 these crystals. The common response can be explained only if the TO_4 tetrahedron is the only
337 major control on the temperature dependence of FWHM for Q^0 crystals.

338 Figure 6a illustrates that the crystals containing Ba and Sr plot lower on Figure 6a than do
339 those containing the lighter elements, Li and Mg. Apparently, the metal in the first coordination
340 sphere of the TO_4 tetrahedra (T = Si, P, S) influences the *absolute values* of FWHM, although
341 they do not affect temperature dependences (Fig. 6b). A mass effect (via Hooke's Law) might be

expected to affect Raman shifts but it is not certain how it would affect FWHM as shown in Figure 6a. Perhaps the cation affects the Heisenberg (natural) lifetime ($FWHM^H$ of Eq. 8a) as proposed for Li_2SiO_3 (Fig. 3a), with the lighter elements decreasing the lifetime of the virtual state thereby increasing FWHM. The possibility requires exploration. Also, the *temperature dependence* of the Q^0 and Q^2 species FWHM is independent both of the type of cation coordinated to the tetrahedron and of the nature of the central element of the tetrahedron. The crystal structures have little effect on Q^0 and Q^2 linewidths. There remains, however, ambiguity as to how cations in the first coordination spheres of tetrahedra affect FWHM.

RELATIONSHIP BETWEEN RAMAN SHIFT AND FWHM

Theoretical Aspects

The second and third terms of the right-hand side of Equation (2) and the first and second terms of Equations (4) and (8a) are identical, although the coefficients of these terms differ. Rearrangement of Equation (2) to isolate the last term yields:

$$[1 + 3/(e^y - 1) + 3/(e^y - 1)^2] = \{\Omega(T) - \omega^* - C[1 + 2/(e^x - 1)]\}/D \quad (9)$$

Its substitution into Equation (4 or 8a), rearrangement and collection of terms gives:

$$FWHM(T) = Q[\Omega(T)] + R[2/(e^x - 1)] + S \quad (10)$$

where Q, R and S are constants with Q = B/D, R = (A – BC/D) and S = (A – (B/D)ω* – BC/D). Equation (10) demonstrates that the FWHM of a Raman band is directly related to its Raman shift. The second term (i.e., $R[2/(e^x - 1)]$) represents the thermal effect on FWHM arising from the nature of the potential energy associated with the symmetric stretch of TO_4. As apparent from Figures 2, 3 and 5 (dashed curves) the slope of the second term is zero at T = 0.0 K. At higher temperature where the energy of the oscillator is greater than kT, (~300 K) the second term contributes linearly to the Raman shift and to FWHM. A consequence is that FWHM plotted

against Raman shift should produce a *linear trend* provided temperatures are greater than about 298 K. The relationship between FWHM(T) and Ω(T) for the four Q^2 silicates and the Q^0 silicate (Mg_2SiO_4) is illustrated in Figure 7. Straight lines of slope -1.0 are superimposed on each trend and they reproduce reasonably well the experimental data regardless of composition or type of Q species (note that the Mg_2SiO_4 data are shifted to fit on the diagram). The straight line relationship predicted from Equation (10) thus is realized at temperatures above ~298 K. The relationship allows for reasonably accurate estimates of FWHM at high temperature provided the Raman shift and FWHM are known at one temperature. Using $CaSiO_3$ as example, consider the 298 K datum point (Fig. 7). With this point and a straight line of slope -1.0, the relationship between Raman shift and FWHM is accurately estimated. To obtain an estimate of FWHM of, for example, $CaSiO_3$ at 1100 K, turn to Figure 2b. At 1100 K, the Raman shift of $CaSiO_3$ is ~969 cm^{-1}. In Figure 7, a Raman shift of 969 cm^{-1} corresponds to a FWHM of ~23 cm^{-1}, which is the FWHM forecast for 1100 K. A reasonable estimate of ω*, the Einstein frequency, can also be made provided the Raman shift and FWHM are known at one temperature. Knowing one point on Figure (7) and extending the slope = -1.0 to absolute zero yields ω* (e.g., dashed line for $CaSiO_3$, bottom of Fig.7). Inspection of Figure 7 indicates slight (concave-upward) curvature to the experimental data of diopside, $CaSiO_3$ and Mg_2SiO_4 (forsterite). The curvature suggests a small additional contribution to the site potential energy (Eq. 1).

Relationships to Other Properties and Phases

From Figure (6a), the cation in the first coordination sphere of TO_4 apparently affects the FWHM of Q species bands, with lighter cations producing broader Q^0 bands. This is attributed to increased lifetime broadening induced by the lighter cations. The data of Figure (6a), when standardized to FWHM value at 298 K (Fig. 6b), yield a common trend demonstrating that the

388 *temperature dependence* of these FWHM are independent of the mass of first coordination
389 sphere cations and are controlled solely by properties of TO_4 (T = Si, P, S). An implication is
390 that all Raman FWHM associated with the symmetric stretch in crystals are controlled by
391 interactions within individual tetrahedra of the unit cell, thus FWHM of glasses and melts may
392 be calculated considering only the array of distinct tetrahedra in these states of matter.

393 Several papers from crystal structures of silicates and sulfates support the control of the
394 "local TO_4 environment" interpretation (e.g., Gibbs, 1982; Downs et al., 1992; Bartelmehs et al.,
395 1995; Jacobsen et al., 1998; Antao, 2012). These studies show that for many silicates and
396 sulfates, similar vibrational T-O motion is expected *regardless* of composition of the crystal or
397 its overall structure. Indeed, the Si-O and S-O bond lengths vary little with composition,
398 structure, or temperature and many of the TO_4 tetrahedra display rigid body thermal motion, with
399 the O-T-O librational angles (θ_L) controlling the size of the thermal ellipsoids. The θ_L at 300 K
400 for different structures (e.g., the Q^0 species in olivine, the Q^2 species in pyroxenes, and the Q^3
401 species in talc), is similar at 2.8°- 3.5º, 3.0°- 3.6° (with the exception of $LiFeSi_2O_6$ at 5.0 - perhaps
402 the reason why Li_2SiO_3 has a larger FWHM than for other silicates), and 4.0°, respectively
403 (Bartelmehs et al., 1995). In addition, θ_L increases greatly with temperature (Fig. 2, Bartelmehs
404 et al., 1995; Armbruster and Geiger, 1993), which again is consistent with the increase in Raman
405 FWHM with temperature.

406 The larger θ_L values for quartz and feldspars of >5 at 300 K (Bartelmehs et al., 1995) are
407 consistent with the large increase in FWHM with temperature, resulting from the A_1 symmetric
408 stretch of quartz. The FWHM of the 464 cm^{-1} and 1084 cm^{-1} A_1 bands in quartz at 300 K ≤ are 7-
409 8 cm^{-1} (Dean et al., 1982; Schmidt and Ziemann, 2000; Ranieri et al., 2009), and these are
410 similar to the FWHM at 300 K for the TO_4 species here addressed (Table 1, Figs.1a, 1b).

411 However at high temperatures, these quartz FWHM increase non-linearly to ~35 cm^{-1} at ~900 K
412 (Schmidt and Ziemann, 2000) and ~40 cm^{-1} at ~1100 K (Ranieri et al., 2009), compared to ≤ 20
413 cm^{-1} at 1200 K for the TO_4 compounds with Na and Ca cations (Figs. 1a,b). Thus, there is good
414 evidence that the libration of the TO_4 tetrahedron alone is a major factor for determining the
415 temperature dependence of the FWHM.

416 A few other qualitative observations are worth mentioning. The FWHM at 300 K for the
417 high energy symmetric A_{1g} or A_g M-X stretch (M=Mg, Sn, P, Mo; X=F,O) for MgF_2, SnO_2, α-
418 $GaPO_4$, $PbMoO_4$ are 4 cm^{-1}, 10 cm^{-1}, ~10cm^{-1}, 13 cm^{-1} respectively compared to the ~10 cm^{-1} for
419 most of the silicates, phosphates and sulfates compiled here (Table 1, Fig.1) More importantly,
420 the temperature dependence of these FWHM are often similar to ours (e.g., Figs. 3c, 6c). For
421 example, MgF_2 yields a FWHM of 23 cm^{-1} at 900 K, compared to the average of ~18 cm^{-1} from
422 the data of Figure 2c. We emphasize, however, that we have focussed on Q^0 and Q^2 A_1 stretching
423 modes. Other vibrational modes can yield very different FWHM and different temperature
424 dependences of the FWHM. Three different vibrational Raman bands of quartz (Dean et al.,
425 1982), for example, produce FWHM that differ by a factor of three and greater, both at 100 K
426 and 300 K. Finally, the temperature dependences of Raman shifts and FWHM of some TO_4
427 species do not behave as described here. The temperature dependence of the Raman shift of the
428 symmetric MoO_4 stretch from ~100 K to 450 K is large at +20 cm^{-1} for $PbMoO_4$ Sinagawa et al.,
429 2000), whereas the change in FWHM over the same temperature range is about -11 cm^{-1}. Clearly
430 the temperature dependences of Raman shift and FWHM are different than shown in Figure 7.

431 **IMPLICATIONS AND CONCLUSIONS**

432 These results answer the questions posed in the Introduction. Lineshapes of crystals are
433 mostly 100% Lorentzian (e.g., Balkanski et al., 1983; Richet et al., 1998; 1996) and their Raman

434 shifts describe unique temperature trends (Figs. 2, 4, 5) primarily because Einstein frequencies
435 (ω^*) differ for the A_1 vibrational mode of each Q species. They vary between ~970-1017 cm^{-1}
436 for the Q^2 crystals studied and ω^* is ~859 cm^{-1} for forsterite (Q^0 crystal). The full width at half
437 maxima (FWHM) also describe unique temperature trends (Figs. 3, 4, 6) due mostly to different
438 Heisenberg lifetimes of the virtual states ($FWHM^H$); apparently the lighter cations causes virtual
439 state lifetimes to decrease, thus increasing FWHM.

440 Standardized Raman shifts display a common trend with respect to temperature (Figs. 2c,
441 4b, 5c) as do standardized FWHM (Figs. 3c, 4d, 6c). The explanation for both trends lies in the
442 origin of the temperature dependence. The harmonic and anharmonic contributions of TO_4
443 common to all crystals studied apparently are similar and effectively independent of either the
444 nature of the element centering the tetrahedron (Si, P. S) or of the nature of the cation in the first
445 coordination sphere of the tetrahedron (Li, Na, Mg, Ca, Sr or Ba). The Balkanski formalism
446 (Balkanski et al., 1983) provides the insight and the explanation for Raman shifts and FWHM
447 temperature trends; they are dependent primarily on the properties of the tetrahedron and virtual
448 (excited) state. Specifically, the temperature dependence of the standardized Raman shifts and
449 FWHM are similar for the seven crystals here considered. The crystals are of different
450 composition and structure, with the only common feature being the TO_4 moiety. The similarities
451 in Raman shift and FWHM displayed by these crystals must arise primarily from the properties
452 of this moiety. The shifts and FWHM for *all crystals* show a strong negative correlation in that
453 the shifts decrease by~30 cm^{-1} whereas the FWHM increase by about 30 cm^{-1} FWHM from 298
454 K to ~1600 K, illustrating the influence of the TO_4 moiety on temperature dependence of Raman
455 shifts and FWHM. This observation is entirely consistent with the theory of Balkanski et al.
456 (1983) modified to include Heisenberg lifetimes (Eq. 8). It is now possible to predict the shift or

457 linewidth for any TO_4 symmetric stretch to within ±5 cm^{-1} up to ~1600 K provided the Raman
458 shift and FWHM are known at 298 K. This remarkable regularity of Raman shifts, FWHM, and
459 their temperature dependences, regardless of composition or crystal structure makes it very likely
460 that local TO_4 tetrahedra and their associated first coordination sphere of cations are the major
461 controls on Q species Raman bands in crystals.

462 ACKNOWLEDGMENTS

463 The authors acknowledge logistical support provided by their associated Universities. We
464 thank Dr. Yang Song for sending us papers on phosphates by Zhai and associates. The authors
465 are especially thankful to the managing editor, Dr. Sergio Speziale, Dr. Charles LeLosq and
466 another reviewer for their detailed editing of the manuscript. The manuscript has been improved
467 greatly due primarily to their efforts.

468 **References**

469 Adamson, A.W. (1973) A Textbook of Physical Chemistry. Academic Press, New York, 1079 p.

470 Antao, S.M. (2012) Structural trends for celestite ($SrSO_4$), anglesite ($PbSO_4$), and barite
471 ($BaSO_4$): Confirmation of expected variations within the SO_4 groups. American
472 Mineralogist, 97, 661-665.

473 Armbruster, T, and Geiger, C.A. (1993) Andradite crystal chemistry, dynamic site disorder and
474 structural strain in silicate garnets. European Journal of Mineralogy, 5, 59-71.

475 Balkanski, M., Wallis, R.F., and Haro, T. (1983) Anharmonic effects in light scattering due to
476 optical phonons in silicon. Physical Review, 28, 1928-1934.

477 Bancroft, G.M., Nesbitt, H.W., Henderson, G.S., O'Shaughnessy, C., Withers, A.C., and
478 Neuville, D.R. (2018) Lorentzian dominated lineshapes and linewidths for Raman
479 symmetric stretch peaks (800-1200 cm^{-1}) in Q species of alkali silicate glasses/melts.

480 Journal of Non-Crystalline Solids, DOI 10.1016/j.jnoncrysol.2018.01.018.

481 Bartelmehs, K.L., Downs, R.T., Gibbs, G.V., Boisen, M.B., Birch, J.B. (1995) Tetrahedral rigid-
482 body motion in silicates. American Mineralogist, 80, 680-690.

483 Bernstein, E.R., Meredith, G.R. (1977) Raman spectra of SiF_4 and GeF_4 crystals. Journal of
484 Chemical Physics, 67, 4132-4138.

485 Bouhfid, M.A., Gruener, G., Mysen, B.O., and Richet, P. (2002) Premelting and calcium
486 mobility in gehlenite ($Ca_2Al_2SiO_7$) and pseudowollastonite ($CaSiO_3$). Physics and
487 Chemistry of Minerals, 29, 655-662.

488 Burke, H.H., and Herman, I.P. (1993) Temperature dependence of Raman scattering in $Ge_{1-x}Si_x$
489 alloys. Physical Review B, 48, 15 016 - 15 024.

490 Cazzanelli, E., and Frech, R. (1984) Temperature dependent Raman spectra of monoclinic and
491 cubic Li_2SO_4. Journal of Chemical Physics, 81, 4729-4736.

492 Cui, J.B., Amtmann, K., Ristein, J., and Ley, L. (1998) Noncontact temperature measurements of
493 diamond by Raman scattering spectroscopy. Journal of Applied Physics, 83, 7929-7933.

494 Dean, K.J., Sherman, W.F., and Wilkinson, G.R. (1982) Temperature and pressure dependence
495 of the Raman active modes of vibration in α-quartz. Spectrochimica Acta, 38A, 1105-
496 1108.

497 Dimanov, A., and Ingrin, J. (1995) Premelting and High-Temperature Diffusion of Ca in
498 Synthetic Diopside: An Increase of the Cation Mobility. Physics and Chemistry of
499 Minerals, 22, 437-442.

500 Dimanov, A., and Jaoul, O. (1998) Calcium self-diffusion in diopside at high temperature:
501 implications for transport properties. Physics and Chemistry of Minerals, 26, 116-127.

502 Downs, R.T., Gibbs, G.V., Bartelmehs, K.L., Boisen, M.B., 1992. Variations of bond lengths and

503 volumes of silicate tetrahedra with temperature. American Mineralogist, 77, 751-757.
504 Efimov, A.M. (1999) Vibrational spectra, related properties, and structure of inorganic glasses.
505 Journal of Non-Crystalline Solids, 253, 95-118.
506 Gibbs, G.V. (1982) Molecules as models for bonding in silicates. American Mineralogist, 67,
507 421-450.
508 Hart, T.R., Aggarwal, R.L., and Lax, B. (1970) Temperature dependence of Raman scattering in
509 silicon. Physical Review B, 1, 638-642.
510 Jacobsen, S.D., Smyth, J.R., Swope, R.J., and Downs, R.T. (1998) Rigid-body character of the
511 SO4 groups in celestine, anglesite and barite. Canadian Mineralogist, 36, 1053-1060.
512 Kingma, K.J., and Hemley, R.J. (1994) Raman spectroscopic study of microcrystalline silica.
513 American Mineralogist, 79, 269-273.
514 Klemens, P.F. (1966) Anharmonic decay of optical photons. Physical Review, 148, 845-848.
515 Kolesov, B.A., and Geiger, C.A., (2004) A Raman spectroscopic study of Fe-Mg olivines.
516 Physical Chemistry of Minerals, 31, 142-154.
517 Liu, M.S., Bursill, L.A., Prawer, S., and Nugent, K.W. (1999) Temperature dependence of
518 Raman scattering in single crystal GaN films. Applied Physics Letters, 74, 3125-3127.
519 Liu, M.S., Bursill, L.A., Prawer, S., and Beserman, R. (2000) Temperature dependence of the
520 first-order Raman phonon line of diamond. Physical Review B, 61, 3391-3395.
521 Loudon, R. (1963) Theory of the first-order Raman effect in crystals. Proceedings of the Royal
522 Society of London A, 275, 218-232.
523 McKeon, D.A., Bell, M.A., and Caracas, R., (2010). Theoretical determination of the Raman
524 spectra of single-crystal forsterite (Mg_2SiO_4). American Mineralogist, 95, 980-986.
525 McMillan, P.F., and Wolfe, G.H. (1995) Vibrational Spectroscopy of Silicate Liquids. Chapter 8

526 in Reviews of Mineralogy and Geochemistry, (ed., P. Ribbe), Mineralogical Society of
527 America, 32, 191-246.
528 Menéndez, J., and Cardona, M. (1984) Temperature dependence of the first-order Raman
529 scattering by phonons in Si, Ge, and α-Sn: Anharmonic effects. Physical Review B, 29,
530 2051-2059.
531 Mohanen, K., Sharma, S.K., and Bishop, F.C. (1993) A Raman spectral study of forsterite-
532 monticellite solid solutions. American Mineralogist, 78, 42-48.
533 Moura, J.V.B.,, da Silva Filho, J.G., Freire, P.T.C., Luz-Lima,C., Pinheiro,G.S., Viana, B.C.,
534 Mendes Filho,J., Souza-Filho, A.G., and Saraiva, G.V. (2016) Phonon properties of β-
535 Ag_2MoO_4: Raman spectroscopy and *ab initio* calculations. Vibrational Spectroscopy, 86,
536 97-102.
537 Nakamura,M., Orihara, H., Ishibashi, Y., Kim, P., and Hirano, S. (1990) Raman scattering of
538 study of gallium orthophosphate (α-$GaPO_4$)- temperature and pressure dependences.
539 Journal of the Physics Society of Japan, 59, 1831-1834.
540 Nesbitt, H.W., Bancroft, G.M., Henderson, G.S., Richet, P., and O'Shaughnessy, C. (2017a)
541 Melting, Crystallization, and the Glass Transition: Toward a Unified Description for
542 Silicate Phase Transitions. American Mineralogist, 102, 412-420.
543 Nesbitt, H.W., Henderson, G.S., Bancroft, G.M., and O'Shaughnessy, C. (2017b) Electron
544 densities over Si and O atoms of tetrahedra and their impact on Raman stretching
545 frequencies and Si-NBO force constants. Chemical Geology, 461, 65-74.
546 Nesbitt, H.W., Cormack, A.N., and Henderson, G.S. (2018) Defect Contributions to the Heat
547 Capacities and Stabilities of Chain, Ring and Sheet Silicates, with Implications for
548 Mantle Minerals. American Mineralogist, doi.org/10.2138/am-2017-6103.

549 Nishidate, K., and Sato, T. (1992) Temperature dependence of the linewidth of the first order
550 Raman spectrum of a MgF_2 crystal. Physical Review B, 46, 13773-13778.
551 Omar, M.A. (1975) Elementary Solid State Physics: Principles and Applications. Addison-
552 Wesley Publishing Co. Reading, Mass. p.76-77.
553 Park, K. (1967) Thermal variation of a Raman line width in calcite. Physics Letters, 25A, 490-
554 491.
555 Popovic, L., Manoun, B., de Waal, D., Nieuwoudt, M.K., and Comins, J.D. (2003) Raman
556 spectroscopic study of phase transitions in Li_3PO_4. Journal of Raman Spectroscopy, 34,
557 77-83.
558 Ranieri, V., Bourgogne, D., Darracq, S., Cambon, M., Haines, J., Cambon, O., Leparc, R.,
559 Lecelut, C., Largeteau, A., and Demazeau, G. (2009) Raman scattering study of α-quartz
560 and $Si_{1-x}Ge_xO_2$ solutions. Physical Review B, 79, 224304 (1-9).
561 Richet, P., Mysen, B.O., and Andrault, D. 1996. Melting and premelting of silicates: Raman
562 spectroscopy and X-ray diffraction of Li_2SiO_3 and Na_2SiO_3. Physics and Chemistry of
563 Minerals, 23,157-172.
564 Richet, P., Mysen, B.O., and Ingrin, J. (1998) High temperature X-ray diffraction and Raman
565 spectroscopy of diopside and pseudowollastonite. Physics and Chemistry of Minerals, 25,
566 401-404.
567 Sadykov, S. (2004) Experimental researches of Na and Pb metaphosphates with high-
568 temperature Raman spectroscopy. Herald of the Department of Earth Sciences RAS 22,
569 1-2.
570 Sato, T., and Asari, T. (1995) Temperature dependence of the linewidth of the first-order Raman
571 spectrum for SnO_2 crystal. Journal of the Physics Society of Japan, 64, 1193-1199.

572 Schmidt, C., and Zieman, M.A. (2000) In-situ Raman spectroscopy of quartz: A pressure sensor
573 for hydrothermal diamond-anvil cell experiments at elevated temperatures. American
574 Mineralogist, 85, 1725-1734.
575 Sinagawa, T., Suda, J., Sato, T., and Saito, H. (2000) Lattice Dynamics and Temperature
576 dependence of the first-order Raman spectra for $PbMoO_4$ crystals. Journal of the Physics
577 Society of Japan, 69, 464-472.
578 Suda, J., Kamishima,O., Kawamura, J., Hattori, T., and Omiya, M. (2014) Phonon anharmonicity
579 of phonon band gap effect of scheelite $PbWO_4$ studied by Raman spectrometry and first-
580 principles calculations. Solid State Communications, 192, 36-41.
581 Swamy,V., Dubrovinsky, L.S., and Matsui, M. (1997) High-temperature Raman spectroscopy
582 and quasi-harmonic lattice dynamic simulation of diopside. Physics and Chemistry of
583 Minerals, 24, 440-446.
584 Voronko, Yu.K., Sobol, A.A., and Shukshin, V.E. (2005) Structure of vanadium-Oxygen and
585 phosphorus-Oxygen groups in molten alkali and alkaline-earth vanadates and phosphates:
586 a high tempertaure Raman scattering study. Inorganic Materials, 41, 1243-1253.
587 Voronko, Yu.K., Sobol, A.A., and Shukshin, V.E. (2006) Raman spectra and structure of silicon-
588 oxygen groups in crystalline, liquid, and glassy Mg_2SiO_4. Inorganic Materials, 42, 981-
589 988.
590 Voronko, Yu.K., Sobol, A.A., Shukshin, V.E., and Gerasymov, I. (2015) Structure and phase
591 transitions of rare-earth pyrosilicates studied by Raman spectroscopy. Inorganic
592 Materials, 51, 1039-1046.
593 Wang, W., Chen, Z., Zhang, F., Saito, K., Tanaka, T., Nishio, M., and Guo, Q. (2016)
594 Temperature dependence of Raman scattering in β-$(AlGa)_2O_3$ thin films. AIP Advances,

6, 015111 (1-10).

Xue, W., Liu, A., Song, Y., and Zhai, S. (2012) High-pressure Raman spectra of Sr-substituted γ-$Ca_{3-x}Sr_x(PO_4)_2$. High Pressure Research, 1, 1-7.

You, J., Jiang, G., and Xu, K. (2001) High temperature Raman spectra of sodium disilicate crystal, glass and its liquid. Journal of Non-Crystalline Solids, 282, 125-131.

Zhai, S., Xue, W., Lin, C-C., Wu, X, and Ito, E. (2011) Raman spectra and X-ray diffraction of tuite at various temperatures. Physics and Chemistry of Minerals, 38, 639-646.

Zhai, S., Lin, C-C., and Xue, W. (2014) Raman spectra of $Sr_3(PO_4)_2$ and $Ba_3(PO_4)_2$ orthophosphates at various temperatures. Vibrational Spectroscopy, 70, 6-11.

Zucker, R. and Shim, S-H. (2009) In situ spectroscopy of $MgSiO_3$ enstatite up to 1550K. American Mineralogist, 94, 1638-1646.

Figure Captions

1. Illustrates the dominant bands of numerous polymorphs of crystalline SiO_2. (a) illustrates the dominant band of α-cristobalite (dots) with a Gaussian and a Lorentzian peak fitted to the upper portion of the low frequency side of the band. (b) illustrates the major band of other SiO_2 polymorphs. The figure is redrawn after Kingma and Hemley (1994).

2. Temperature dependence of the Raman peak shifts (cm^{-1}) for the SiO_4 symmetric stretch peak in the four metasilicate minerals containing the Q^2 species (Richet et al., 1996, 1998). a) Li_2SiO_3 (shaded circles) and Na_2SiO_3 (solid black circles); b) $Ca_{0.5}Mg_{0.5}SiO_3$ (open triangles), and $CaSiO_3$ (open squares); c) Raman shifts for all four silicates standardized to the the value at 298 K. The errors bars are all $\pm 1 cm^{-1}$. Best fits using eq.(2) are shown with solid black lines, with the dashed lines showing the contribution from the second (quartic) term (the D term) to the Raman shift. The best fit values for the constants ω*, C

and D for the four minerals are shown in the figures.

3. Temperature dependence of the FWHM (Full Width at Half Maximum, in cm^{-1}) for the SiO_4 symmetric stretch peak of same Q^2 crystals as in Figure 2. a) Li_2SiO_3 (shaded circles) and Na_2SiO_3 (solid black circles). Dashed curves illustrate the contribution of the quadratic term (i.e., $A[2/(e^x - 1)]$) of Equation (8a) to temperature dependence; b) $CaSiO_3$ (solid black circles) and $Ca_{0.5}Mg_{0.5}SiO_3$ (shaded circles); c) linewidths for the above four silicates standardized to the Raman linewidth at 298K set to 0 cm^{-1}. Error bars are all ±2 cm^{-1}. The solid curve is the best fit to all plotted data using Equation (8a). The best fit values for the constants FWHM*, A and B are provided in the figures.

4. Temperature dependence of the Raman shift and FWHM for the SiO_4 symmetric stretch peak in the Q^0 species Mg_2SiO_4 (Kolosev and Geiger 2004) compared to the shifts and FWHM for other Q^0 and Q^2 species: a) the Raman shifts for Mg_2SiO_4 (black circles) along with best least squares linear fit to the data; b) the standardized shifts [$\Omega(T)$ - $\Omega(298)$] for Mg_2SiO_4 compared to the standardized shifts for the Q^0 species Li_3PO_4 (open squares), and the Q^2 species $CaSiO_3$(open diamonds). The errors bars are all ± 1cm^{-1}; c) the FWHM for Mg_2SiO_4 compared to the FWHM for $CaSiO_3$, and the best least squares linear fit for Mg_2SiO_4 is shown. The errors bars are all ±2 cm^{-1} in c); d) the FWHM standardized to the linewidth at 298 K at 0 cm^{-1} for Mg_2SiO_4 compared to those for the four metasilicates shown earlier in Fig. 2c. In d), the FWHM for Na_2SiO_3 for five values in the premelting region (1259K-1348K cm^{-1}) are again omitted - see text.

5. Temperature dependence of the Raman peak position (cm^{-1}) for the TO_4 (T = Si, P, S) symmetric stretch peak for Q^0 species in Li_2SO_4 (Cazzanelli and Frech 1984), Li_3PO_4 (Popovic et al., 2003), and Mg_2SiO_4 (Kolosev and Geiger, 2004) compared to Li_2SiO_3

(with Q^2 species) previously shown in Fig. 1a. a) Li_2SO_4 (open circles), and Li_2SiO_3 (solid black circles); b) Li_3PO_4 (open circles) and Li_2SiO_3 (solid black circles); c) positions for all the three crystalline minerals compounds, along with the positions for Mg_2SiO_4 (black circles) from Fig. 4a standardized to the peak position at 298K ($\Omega(T) - \Omega(298)$). The errors bars are ± 1$cm^{-1.}$ The best fits in Fig.5a, 5b using Equation (2) and the best fit values for the constants ω*, C and D are shown with solid black lines, with the dashed lines showing the contribution from the second (quartic) term to the Raman shift. The solid line in Fig. 5c is from a quadratic fit just to guide the eye.

6. Temperature dependence of the FWHM in cm^{-1} for the TO_4 (T=Si, P, S) symmetric stretch peak for Q^0 species in Li_2SO_4 (Cazzanelli and Frech 1984), Li_3PO_4 (Popovic et al., 2003) $Ba_3(PO_4)_2$ and $Sr_3(PO_4)_2$ (Zhai et al., 2014) and Mg_2SiO_4 (Kolosev and Geiger 2004). a) Li_2SO_4 (open circles), Li_3PO_4 (open diamonds), $Ba_3(PO_4)_2$ (shaded circles) and $Sr_3(PO_4)_2$ (open diamonds), and Mg_2SiO_4 (solid black circles) ; b) FWHM for the five Q^0 compounds standardized to the Raman linewidth at 298K taken as 0 cm^{-1}. The error bars are ± 2 cm^{-1}. c) standardized FWHM for the phosphates and Mg_2SiO_4 compared to the standardized FWHM for $CaSiO_3$ (shaded diamonds).

7. Plots of FWHM versus Raman shift (Ω) for the five silicates- four Q^2 species (Li_2SiO_3, Na_2SiO_3, $CaSiO_3$, $Ca_{0.5}Mg_{0.5}SiO_3$) and one Q^0 species (Mg_2SiO_4). The five lines (all with a slope of -1) are drawn to guide the eye so that most of the data is close to the line for a given mineral. Note that the Mg_2SiO_4 trend is offset by 135 cm^{-1} to greater Ω(T) values to include the trend on this plot. The temperature increases from the far bottom right to the far upper left for each of the five minerals, as is indicated by the 298K for $Ca_{0.5}Mg_{0.5}SiO_3$ and Mg_2SiO_4(bottom right) to the highest temperatures (1667K for

665 $Ca_{0.5}Mg_{0.5}SiO_3$ and 1145K for Mg_2SiO_4. Note the ω* value (992 cm-1) for $CaSiO_3$,
666 obtained from the extrapolation of the line to 0 FWHM. This is slightly higher than the
667 ω* value obtained in Fig. 1b (987.6 cm^{-1}).
668

669

Table 1: Raman Shifts and FWHM for the SiO_4 Symmetric Stretch of Crystals

Crystal	Species	Temp. = 298K		Temp ~1200K		Reference
		Shift	FWHM	Shift	FWHM	
		cm^{-1}	cm^{-1}	cm^{-1}	cm^{-1}	
Mg_2SiO_4	Q^0	856	8	824	23	Kolosev and Geiger, (2004)
	Q^0	856	<10	826		McKeon et al., (2010)
	Q^0	855		830	20	Voronko et al. (2006)
$CaMgSiO_4$	Q^0	850	10	816		Mohanan et al., (1993)
$Gd_2Si_2O_7$	Q^1	915	<10	902	~30	Voronko et al., (2015)
$MgSiO_3$	Q^2	1036	12	1014	22	Zucker and Shim, (2009)
Na_2SiO_3	Q^2	965	6	950	27	Richet et al., (1996)
Li_2SiO_3	Q^2	975	13	960	26	Richet et al., (1996)
$Ca_{0.5}Mg_{0.5}SiO_3$	Q^2	1008	10	988	24	Richet et al., (1998)
	Q^2	1014	7			Swamy et al., (1997)
$CaSiO_3$	Q^2	981	10	967	26	Richet et al., (1998)
$Na_2Si_2O_5$	Q^3	1072	~5			You et al., (2001)

670

671

672

673

Table 2: Raman Shifts and FWHM for Symmetric Stretch of P and S Crystals

Crystal	Species	Temp. = 298K Shift	FWHM	Temp.	FWHM	Reference
		cm^{-1}	cm^{-1}	K	cm^{-1}	
Li_2SO_4	Q^0	1012	~9.5	~900	20	Cazzanelli and Frech (1984)
$Ca_3(PO_4)_2$	Q^0	980	~9	~1200	21	Zhai et al., (2011)
$Sr_3(PO_4)_2$	Q^0	1080	6	~1200	19	Zhai et al., (2014)
$Ba_3(PO_4)_2$	Q^0	1045	5	~1200	18	Zhai et al., (2014)
$CaSr_2(PO_4)_2$	Q^0	961	~10			Xue et al., (2012)
$Li_3PO_4(\beta,\gamma)$	Q^0	980	6	~1420	30	Voronko et al., (2005)
$Li_3PO_4(\beta,\gamma)$	Q^0	950	11	~1370	34	Popovic et al., (2003)
$Li_4P_2O_7$	Q^1	1050	6	~1200	25	Voronko et al., (2005)
$NaPO_3$	Q^2	1180	6	~850	20	Voronko et al., (2005)
	Q^2	1180	6	~785	20	Sadykov (2004)

674

This is a preprint, the final version is subject to change, of the American Mineralogist (MSA)
Cite as Authors (Year) Title. American Mineralogist, in press.
DOI: https://doi.org/10.2138/am-2018-6314

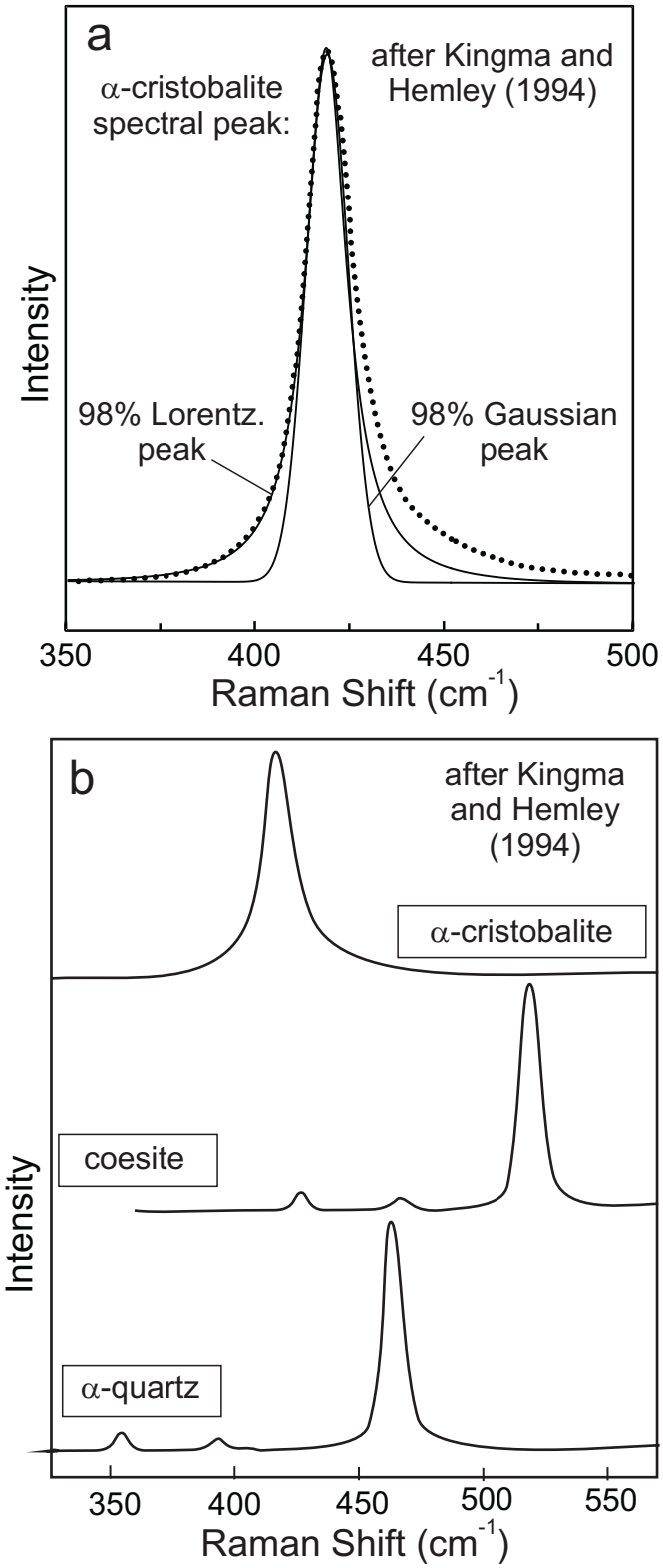

Fig. 1

This is a preprint, the final version is subject to change, of the American Mineralogist (MSA)
Cite as Authors (Year) Title. American Mineralogist, in press.
DOI: https://doi.org/10.2138/am-2018-6314

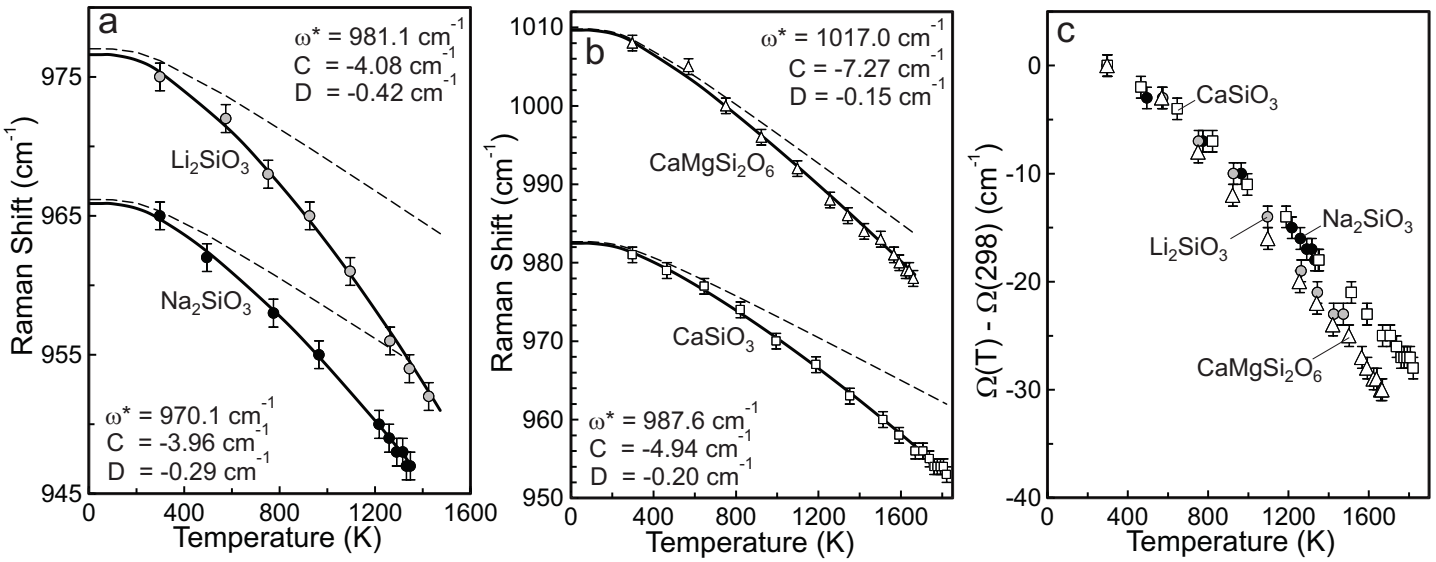

Fig. 2

This is a preprint, the final version is subject to change, of the American Mineralogist (MSA)
Cite as Authors (Year) Title. American Mineralogist, in press.
DOI: https://doi.org/10.2138/am-2018-6314

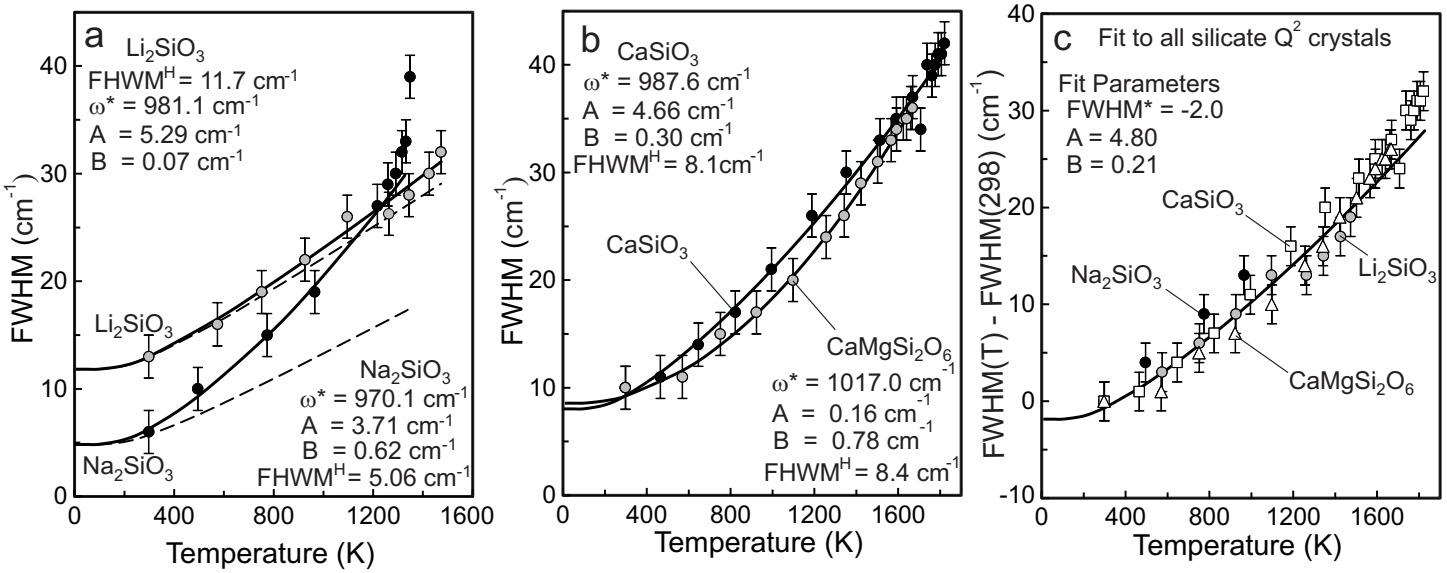

Fig. 3

This is a preprint, the final version is subject to change, of the American Mineralogist (MSA)
Cite as Authors (Year) Title. American Mineralogist, in press.
DOI: https://doi.org/10.2138/am-2018-6314

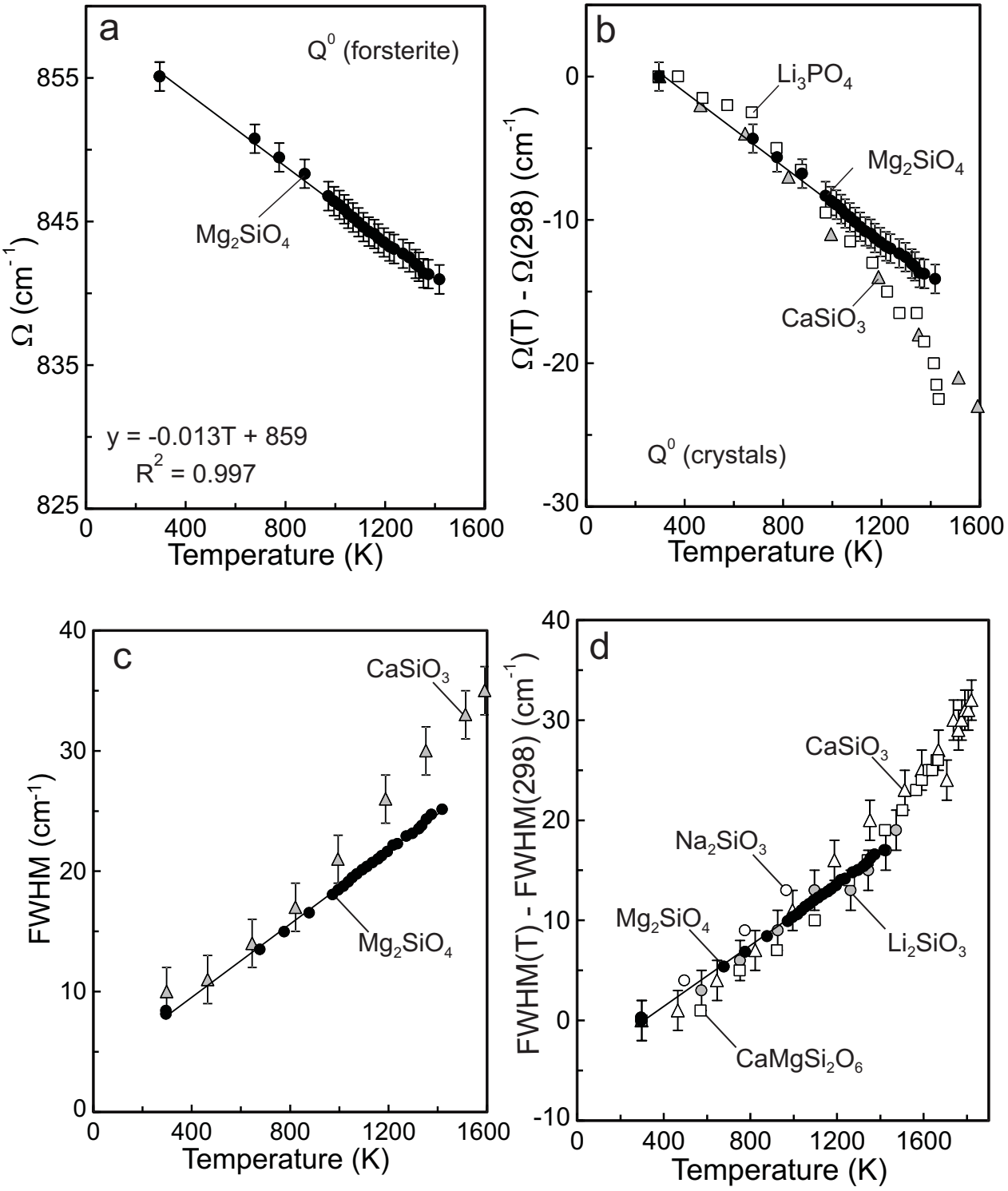

Fig. 4

This is a preprint, the final version is subject to change, of the American Mineralogist (MSA)
Cite as Authors (Year) Title. American Mineralogist, in press.
DOI: https://doi.org/10.2138/am-2018-6314

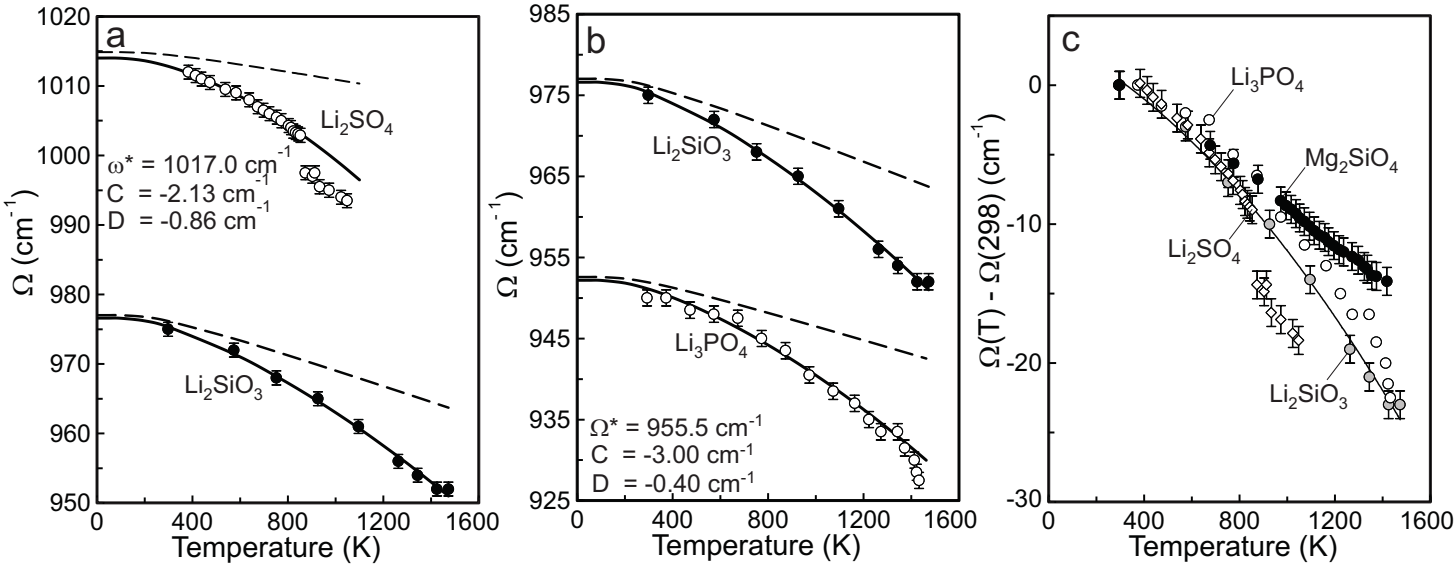

Fig. 5

This is a preprint, the final version is subject to change, of the American Mineralogist (MSA)
Cite as Authors (Year) Title. American Mineralogist, in press.
DOI: https://doi.org/10.2138/am-2018-6314

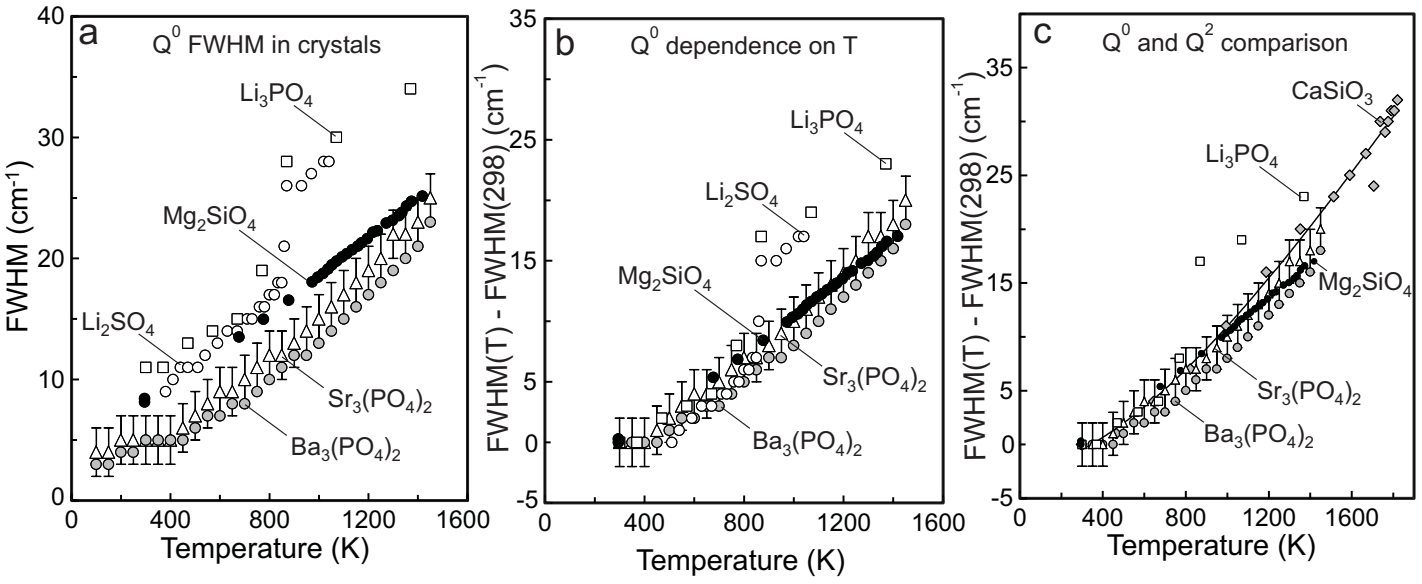

Fig. 6

This is a preprint, the final version is subject to change, of the American Mineralogist (MSA)
Cite as Authors (Year) Title. American Mineralogist, in press.
DOI: https://doi.org/10.2138/am-2018-6314

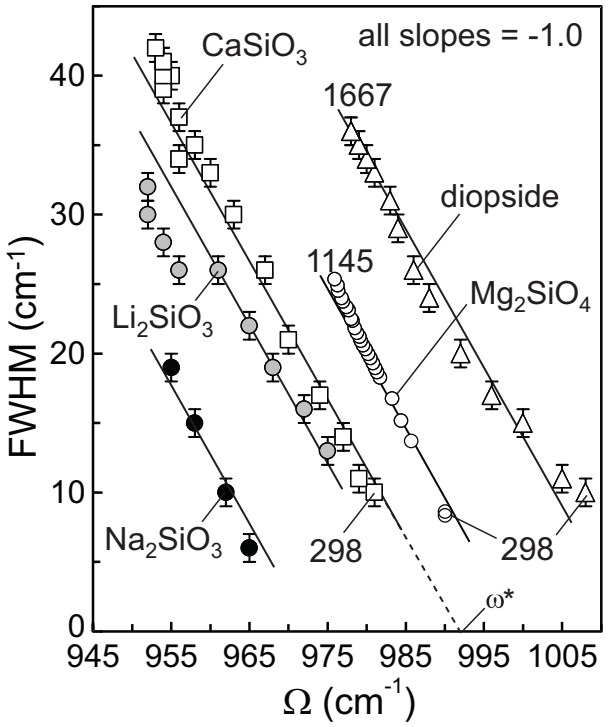

Fig. 7